Published in final edited form as:
Bioconjug Chem. 2009 August 19; 20(8): 1559–1568. doi:10.1021/bc9001739.

2-Mercaptoacetylglycylglycyl (MAG_2) as a Bifunctional Chelator for ^{99m}Tc-Labeling of Cyclic RGD Dimers: Effect of Technetium Chelate on Tumor Uptake and Pharmacokinetics

Jiyun Shi[1,2], **Young-Seung Kim**[1], **Sudipta Chakraborty**[1], **Bing Jia**[2], **Fan Wang**[2], and **Shuang Liu**[1,*]

[1]School of Health Sciences, Purdue University, IN 47907, USA

[2]Medical Isotopes Research Center, Peking University, Beijing 100083, China

Abstract

This report describes the synthesis of MAG_2-PEG_4-E[c(RGDfK)]$_2$ (MAG_2-P-RGD_2: MAG_2 = S-benzoylmercaptoacetylglycylglycyl; PEG_4 = 15-amino-4,7,10,13-tetraoxapentadecanoic acid) and MAG_2-PEG_4-E[PEG_4-c(RGDfK)]$_2$ (MAG_2-3P-RGD_2), and the evaluation of ^{99m}TcO(MAG_2-P-RGD_2) and ^{99m}TcO(MAG_2-3P-RGD_2) as new radiotracers for tumor imaging in the athymic nude mice bearing U87MG human glioma xenografts. We found that MAG_2 is such an efficient bifunctional chelating agent that ^{99m}TcO(MAG_2-P-RGD_2) and ^{99m}TcO(MAG_2-3P-RGD_2) could be prepared in high yield (>90%) with high specific activity (~5 Ci/μmol) using a kit formulation. ^{99m}TcO(MAG_2-P-RGD_2) and ^{99m}TcO(MAG_2-3P-RGD_2) have very high solution stability in the kit matrix. Biodistribution data in athymic nude mice bearing U87MG human glioma xenografts indicated that replacing the highly charged [^{99m}Tc(HYNIC)(tricine)(TPPTS)] (6-hydrazinonicotinyl and TPPTS = trisodium triphenylphosphine-3,3′,3″-trisulfonate) with smaller ^{99m}TcO(MAG_2) resulted in a significant increase in the radiotracer uptake in the tumor and normal organs most likely due to the higher lipophilicity of ^{99m}TcO(MAG_2-3P-RGD_2) (log P = -3.15 ± 0.10) than that for [^{99m}Tc(HYNIC-3P-RGD_2)(tricine)(TPPTS)] (^{99m}Tc-3P-RGD_2: log P = -3.96 ± 0.05). Even though ^{99m}TcO(MAG_2-3P-RGD_2) has better tumor uptake (15.48 ± 2.49 %ID/g at 60 min postinjection (p.i.)) than ^{99m}Tc-3P-RGD_2 (9.15 ± 2.13 %ID/g at 60 min p.i.), its tumor-to-background (T/B) ratios (tumor/blood = 13.02 ± 6.12; tumor/liver = 4.07 ± 0.95; tumor/lung = 2.97 ± 0.64; and tumor/muscle = 8.04 ± 0.43) are not as good as those of ^{99m}Tc-3P-RGD_2 (tumor/blood = 36.0 ± 11.5; tumor/liver = 5.14 ± 1.46; tumor/lung = 4.36 ± 0.54; and tumor/muscle = 13.70 ± 2.21) at 60 min p.i. On the basis of these results, we believe that ^{99m}Tc-3P-RGD_2 remains a better radiotracer because of its higher T/B ratios.

Keywords

integrin $\alpha_v\beta_3$; ^{99m}Tc -labeled cyclic RGD peptides; tumor imaging

Introduction

Radiolabeled cyclic RGD (Arg-Gly-Asp) peptides represent a new class of radiotracers that target the integrin $\alpha_v\beta_3$ overexpressed on both tumor cells and endothelial cells of neovasculature during tumor growth, invasion and metastasis (1-12). Many radiolabeled

*To whom correspondence should be addressed: School of Health Sciences, Purdue University, 550 Stadium Mall Drive, West Lafayette, IN 47907. Phone: 765-494-0236; Fax 765-496-1377; Email: lius@pharmacy.purdue.edu.

cyclic RGD peptides have been evaluated for imaging integrin $\alpha_v\beta_3$-positive tumors by single photon emission computed tomography (SPECT) or positron emission tomography (PET) over the last several years, (13-49). Among the RGD peptide radiotracers evaluated in different tumor-bearing animal models, [^{18}F]-AH111585, the core peptide sequence discovered from a phage display library (such as ACDRGDCFCG) (50,51), and [^{18}F]Galacto-RGD (2-[^{18}F]fluoropropanamide c(RGDfK(SAA); SAA = 7-amino-L-glyero-L-galacto-2,6-anhydro-7-deoxyheptanamide) (52-54) are currently under clinical investigations for noninvasive visualization of integrin $\alpha_v\beta_3$ expression in cancer patients. The imaging studies show that the ^{18}F-labeled RGD peptides are able to target integrin $\alpha_v\beta_3$–positive tumors (51-54). However, the low tumor uptake, high cost and lack of preparation modules for ^{18}F-labeled cyclic RGD peptides impose a significant challenges their continued clinical applications.

To improve integrin $\alpha_v\beta_3$ binding affinity and radiotracer tumor uptake, multimeric cyclic RGD peptides, such as E[c(RGDfK)]$_2$ and E{E[c(RGDfK)]$_2$}$_2$, were used as targeting biomolecules to carry radionuclide (e.g. ^{99m}Tc, ^{18}F, ^{64}Cu, and ^{111}In) to the integrin $\alpha_v\beta_3$ on tumor cells and endothelial cells of the tumor neovasculature (20-22,30-35,37-49). The results from in vitro assays, ex-vivo biodistribution and in vivo imaging studies clearly demonstrate that the radiolabeled (^{99m}Tc, ^{18}F, ^{64}Cu, and ^{111}In) multimeric cyclic RGD peptides, such as E{E[c(RGDxK)]$_2$}$_2$ and E[c(RGDxK)]$_2$ (x = f and y), have better tumor targeting capability as evidenced by their higher integrin $\alpha_v\beta_3$ binding affinity, better tumor uptake with longer tumor retention times than their monomeric counterparts (20-22,30-35,37-49). However, the uptake of radiolabeled (^{99m}Tc, ^{18}F, ^{64}Cu and ^{111}In) multimeric cyclic RGD peptides in the kidneys and liver is also increased as the peptide multiplicity increases.

Recently, we reported the evaluation of the complex [^{99m}Tc(HYNIC-3P-RGD$_2$)(tricine)(TPPTS)] (Figure 1: ^{99m}Tc-3P-RGD$_2$; HYNIC = 6-hydrazinonicotinyl; TPPTS = trisodium triphenylphosphine-3,3′,3″-trisulfonate; 3P-RGD$_2$ = PEG$_4$-E[PEG$_4$-c(RGDfK)]$_2$ and PEG$_4$ = 15-amino-4,7,10,13-tetraoxapentadecanoic acid) as radiotracers for imaging integrin $\alpha_v\beta_3$ expression in athymic nude mice bearing U87MG glioma and MDA-MB-435 breast cancer xenografts (55). The PEG$_4$ linkers are used to increase the distance between two cyclic RGD motifs from 6 bonds (excluding side arms of K-residues) in E[c(RGDfK)]$_2$ to 38 bonds in 3P-RGD$_2$ in so that they are able to achieve the simultaneous integrin $\alpha_v\beta_3$ binding in a bivalent fashion, and to improve radiotracer excretion kinetics from noncancerous organs. Results from the $\alpha_v\beta_3$ integrin binding assay show that the addition of PEG$_4$ linkers between two cyclic RGD motifs makes it possible for 3P-RGD$_2$ to become bivalent in binding to the integrin $\alpha_v\beta_3$. The results from biodistribution studies clearly demonstrate that PEG$_4$ and G$_3$ linkers are useful for improving the tumor uptake and clearance kinetics of ^{99m}Tc radiotracers from noncancerous organs (55,56). Similar results were also obtained for [^{99m}Tc(HYNIC-3G-RGD$_2$)(tricine)(TPPTS)] (^{99m}Tc-3G-RGD$_2$: 3G-RGD$_2$ = G$_3$-E[G$_3$-c(RGDfK)]$_2$ and G$_3$ = Gly-Gly-Gly) (56), ^{64}Cu(DOTA-3P-RGD$_2$) (DOTA = 1,4,7,10-tetraazacyclo-dodecane-1,4,7,10-tetracetic acid) and ^{64}Cu(DOTA-3G-RGD$_2$) (57).

As a continuation of our interest in radiolabeled cyclic RGD peptides as radiotracers for tumor imaging (41-44,55,56), we prepared two novel cyclic RGD conjugates, MAG$_2$-PEG$_4$-E[c(RGDfK)]$_2$ (MAG$_2$-P-RGD$_2$: MAG$_2$ = S-benzoylmercaptoacetylglycylglycyl) and MAG$_2$-3PEG$_4$-E[PEG$_4$-c(RGDfK)]$_2$ (MAG$_2$-3P-RGD$_2$), and their ^{99m}Tc complexes (Figure 1: ^{99m}TcO(MAG$_2$-P-RGD$_2$) and ^{99m}TcO(MAG$_2$-3P-RGD$_2$). MAG$_2$ is of our particular interest as the bifunctional chelator (BFC) because it forms the ^{99m}TcO(MAG$_2$) chelate (molecular weight (MW) ~300 Daltons) that is much smaller than the bulky and highly charged [^{99m}Tc(HYNIC)(tricine)(TPPTS)] (MW ~ 900 Daltons). The integrin $\alpha_v\beta_3$ binding affinities of MAG$_2$-P-RGD$_2$ and MAG$_2$-3P-RGD$_2$ were determined using a displacement

assay against ^{125}I-c(RGDyK) bound to U87MG glioma cells. Biodistribution characteristics of ^{99m}TcO(MAG$_2$-P-RGD$_2$) and ^{99m}TcO(MAG$_2$-3P-RGD$_2$) were evaluated in the athymic nude mice bearing U87MG glioma xenografts. The main objective of this study is to demonstrate the usefulness of MAG$_2$ as a BFC for ^{99m}Tc-labeling of small biomolecules, and to assess the impact of ^{99m}Tc chelates (^{99m}TcO(MAG$_2$) vs. [^{99m}Tc(HYNIC)(tricine)(TPPTS)]) on both tumor uptake and tumor-to-background (T/B) ratios.

Experimental Section

Materials

Chemicals were purchased from *Sigma-Aldrich* (St. Louis, MO), and were used without further purification. Cyclic RGD peptides, PEG$_4$-E[PEG$_4$-c(RGDfK)]$_2$ (3P-RGD$_2$) and PEG$_4$-E[PEG$_4$-c(RGKfD)]$_2$ (3P-RGK$_2$: a scrambled nonsense peptide), were custom-made by the Peptides International, Inc. (Louisville, KY). MAG$_2$ (S-benzoylmercaptoacetylglycylglycine) and PEG$_4$-E[c(RGDfK)]$_2$ (P-RGD$_2$) were prepared according to the literature methods (43,58). Na^{99m}TcO$_4$ was obtained from a commercial DuPont Pharma ^{99}Mo/^{99m}Tc generator (North Billerica, MA). The ESI (electrospray ionization) mass spectral data were collected on a Finnigan LCQ classic mass spectrometer, School of Pharmacy, Purdue University.

HPLC Methods

HPLC Method 1 used a LabAlliance HPLC system equipped with a UV/vis detector (λ=254 nm) and Zorbax C$_{18}$ semi-prep column (9.4 nm × 250 mm, 100 Å pore size; Agilent Technologies, Santa Clara, CA). The flow rate was 2.5 mL/min with the mobile phase starting from 90% A (25 mM NH$_4$OAc, pH = 6.8) and 10% B (acetonitrile) at 0 min, followed by a gradient mobile phase going from 85% A and 15% B at 5 min to 65% A and 35% B at 30 min. The radio-HPLC method (Method 2) used the LabAlliance HPLC system equipped with a β-ram IN/US detector (Tampa, FL) and Zorbax C$_{18}$ column (4.6 mm × 250 mm, 300 Å pore size; Agilent Technologies, Santa Clara, CA). The flow rate was 1 mL/min. The mobile phase was isocratic with 90% A (25 mM NH$_4$OAc, pH = 6.8) and 10% B (acetonitrile) at 0 – 2 min, followed by a gradient mobile phase going from 10% B at 2 min to 15% B at 5 min and to 20% B at 20 min. The radio-ITLC method used GelmanSciences silica-gel paper strips and a 1:1 mixture of acetone and saline as eluant. By this method, ^{99m}Tc-labeled cyclic RGD peptides migrate to the solvent front while ^{99m}TcO$_4^-$ and [^{99m}Tc]colloid remain at the origin.

MAG$_2$-OSu

To a solution of MAG$_2$ (310 mg, 1 mmol) and N-hydroxysuccinimide (130 mg, 1.1 mmol) in DMF (5 mL) was added dicyclcohexylcarbodiimide (DCC: 230 mg, 1.1 mmol). The mixture was stirred at room temperature for 24 h. After addition of 0.3 mL acetic acid, the resulting mixture was stirred at room temperature for another 5 h. The precipitate was filtered, and discarded. The filtrate was evaporated to dryness on a rotary evaporator. The residue was dissolved in dichloromethane (10 mL). After filtration, the filtrate was concentrated to ~2 mL. The solution was added dropwise into diethyl ether (20 mL) to give an off-white precipitate. The solid product was collected, washed with diethyl ether, and dried under vacuum. The yield was 340 mg (83%). ^{1}H NMR (CDCl$_6$, chemical shifts in ppm relative to TMS): 2.81 (s, 4H, *COCH$_2$CH$_2$CO*); 3.78 (s, 2H, *SCH$_2$CO*); 4.03 (d, 2H, *CH$_2$CO*); 4.38 (d, 2H, *CH$_2$CO*); 7.13 (dt, 2H, *aromatic*); 7.47 (t, 2H, *aromatic*); 7.61 (t, H, *aromatic*); and 7.96 (d, 2H, *NH*CO). ESI-MS: m/z = 408.50 for [M+H]$^+$ (408 calcd. for [C$_{17}$H$_{18}$N$_3$O$_7$S]$^+$).

MAG_2-P-RGD_2

MAG_2-OSu (5.8 mg, 14.2 μmol) and P-RGD_2 (5.4 mg, 3.45 μmol) were dissolved in DMF (2 mL). To the mixture above was added diisopropylethylamine (DIEA, 2 drops). The solution was stirred at room temperature for 2 h. After addition of water (2 mL), the pH was adjusted to 3.0 – 4.0. The product was separated from the reaction mixture by HPLC (Method 1). Fractions at 17.5 min were collected. Lyophilization of combined collections afforded the crude product MAG_2-P-RGD_2 (~75% purity by HPLC), which was then further purified by HPLC (Method 2). The yield was 2.7 mg (42%). ESI-MS: m/z = 1858.43 for (1857 calcd. For $[C_{84}H_{121}N_{22}O_{25}S]^+$).

MAG_2-3P-RGD_2

MAG_2-3P-RGD_2 was prepared in a similar fashion as that for MAG_2-P-RGD_2 using MAG_2-OSu (4 mg, 9.7 μmol) and 3P-RGD_2 (5 mg, 2.43 μmol). The product was purified by HPLC (Method 1). Fractions at ~16 min were collected. Lyophilization of the combined collections afforded the crude product MAG_2-3P-RGD_2 (~77% purity by HPLC), which was further purified by HPLC (Method 2). Lyophilization of the combined collections at 20 min afforded MAG_2-3P-RGD_2 with >95% HPLC purity. The yield was 2.0 mg (35%). ESI-MS: m/z = 2351.79 for (2351 calcd. for $[C_{105}H_{163}N_{24}O_{35}S]^+$).

MAG_2-PEG_4-E[PEG_4-c(RGKfD)]$_2$ (MAG_2-3P-RGK_2)

MAG_2-3P-RGK_2 was prepared according to the same procedure used for MAG_2-PEG_4-dimer using MAG_2-OSu (12.5 mg, 40 μmol) and 3P-RGK_2 (15 mg, 7.29 μmol). The product was separated from the reaction mixture by HPLC (Method 1). Fractions at 16 min were collected. Lyophilization of the combined collections afforded the crude product MAG_2-3P-RGK_2 (~70% purity by HPLC), which was then further purified by HPLC (Method 2). Lyophilization of the combined collections at 19 min afforded MAG_2-3P-RGK_2 with >95% HPLC purity. The yield was 6.2 mg (36%). ESI-MS: m/z = 2351.76 for (2351 calcd. for $[C_{105}H_{163}N_{24}O_{35}S]^+$).

^{99m}Tc-Labeling

To a lyophilized vial containing 2.28 mg of NaH_2PO_4, 11.5 mg of Na_2HPO_4, 50 mg of α-D-glucoheptonic acid, 50 μg of $SnCl_2.2H_2O$, and 25 μg of the MAG_2-conjugate (MAG_2-P-RGD_2, MAG_2-3P-RGD_2 or MAG_2-3P-RGD_2) was added 1.0 mL of $Na^{99m}TcO_4$ solution (10 – 50 mCi/mL). The vial was heated at 100 °C for 20 – 25 min in a lead-shielded water bath. After heating, the vial was placed back into the lead pig, and allowed to stand at room temperature for ~10 min. A sample of the resulting solution was analyzed by radio-HPLC (Method 2) and radio-ITLC. The radiochemical purity (RCP) was >95% for all three radiotracers, ^{99m}TcO(MAG_2-P-RGD_2), ^{99m}TcO(MAG_2-3P-RGD_2) and ^{99m}TcO(MAG_2-3P-RGK_2), with less than 0.5% of [^{99m}Tc]colloid.

Dose Preparation

For the ex-vivo biodistribution studies, the ^{99m}Tc radiotracers were first prepared, and were then purified by HPLC (Method 2). Volatiles in the HPLC mobile phases were removed under vacuum. The dose solution was prepared by dissolving the purified radiotracer in saline to a concentration of 10 – 25 μCi/mL. In the blocking experiment, E[c(RGDfK)]$_2$ was dissolved in the dose solution to ~3.5 mg/mL. For imaging studies, ^{99m}TcO(MAG_2-3P-RGD_2) was prepared in high yield (RCP > 95%). Doses were made by dissolving the reconstituted kit solution to a concentration of 5 mCi/mL. The solution was filtered with a 0.20 μ Millex-LG filter to remove any particle or precipitate. Each tumor-bearing mouse was injected with ~0.1 mL of the filtered dose solution.

Determination of Log P Values

Log P values of were determined using the following procedure: the ^{99m}Tc radiotracer was purified by HPLC. Volatiles were removed completely under vacuum. The residue was dissolved in a equal volume (3 mL:3 mL) mixture of n-octanol and 25 mM phosphate buffer (pH = 7.4). After stirring vigorously for ~20 min, the mixture was centrifuged at a speed of 8,000 rpm for 5 min. Samples (in triplets) from n-octanol and aqueous layers were counted in a Perkin Elmer Wizard – 1480 γ-counter (Shelton, CT). The log P value was measured three different times and reported as an average of three independent measurements plus the standard deviation.

In Vitro Whole-Cell Integrin $\alpha_v\beta_3$ Binding Assay

The *in vitro* integrin binding affinity of cyclic RGD peptides were assessed by a displacement assay using ^{125}I-c(RGDyK) as the integrin $\alpha_v\beta_3$-specific radioligand. Experiments were performed on U87MG human glioma cells by slight modification of a method previously described (28,30). Briefly, U87MG glioma cells were grown in Gibco's Dulbecco's medium supplemented with 10% fetal bovine serum (FBS), 100 IU/ml penicillin and 100 μg/ml streptomycin (Invitrogen Co, Carlsbad, CA), at 37 °C in humidified atmosphere containing 5% CO_2. Filter multiscreen DV plates were seeded with 10^5 cells in binding buffer and incubated with ^{125}I-c(RGDyK) in the presence of increasing concentrations of cyclic RGD peptides. After removing the unlabeled c(RGDyK), hydrophilic PVDF filters were collected and the radioactivity was determined using a gamma counter (Packard, Meriden, CT). The IC_{50} values were calculated by fitting the data by nonlinear regression using GraphPad Prism^{TM} (GraphPad Software, Inc., San Diego, CA), and reported as an average plus the standard deviation. Comparison between two radiotracers was made using the two-way ANOVA test (GraphPad Prim 5.0, San Diego, CA). The level of significance was set at $p < 0.05$.

Animal Model

Biodistribution studies were performed using the athymic nude mice bearing U87MG human glioma xenografts in compliance the NIH animal experiment guidelines (*Principles of Laboratory Animal Care*, NIH Publication No. 86-23, revised 1985). The protocol was approved by Purdue University Animal Care and Use Committee (PACUC). The U87MG human glioma cells were grown at 37 °C in Minimal Essential Medium (Alpha Modification) containing 3.7 g of sodium bicarbonate/L, 10% fetal bovine serum v/v, and 5% Penicillin Streptomycin (GIBCO, Grand Island, NY) in a humidified atmosphere of 5% carbon dioxide. Female athymic nu/nu mice were purchased from NCI at 4 – 5 weeks of age. The mice were implanted subcutaneously with ~8×10^6 U87MG human glioma cells into the upper left flanks. All procedures will be performed in a laminar flow cabinet using aseptic technique. Two to three weeks after inoculation, the tumor size was 0.1 – 0.4 g, and animals were used for biodistribution and imaging studies.

Biodistribution Protocol

Fifteen tumor-bearing mice (20 – 25 g) were randomly divided into four groups. Each animal was administered with ^{99m}Tc radiotracer (~2.5 μCi in 0.1 mL saline) via tail vein. Five animals were euthanized by sodium pentobarbital overdose (100 – 200 mg/kg) at 30, 60 and 120 min postinjection (p.i.). Blood samples were withdrawn from the heart. The tumor and normal organs (brain, eyes, heart, intestine, kidneys, liver, lungs, muscle and spleen) were excised, washed with saline, dried with absorbent tissue, weighed, and counted on a γ-counter (Perkin Elmer Wizard – 1480). The organ uptake was calculated as the percentage of injected dose per gram of organ tissue (%ID/g). For the blocking experiment to demonstrate the radiotracer integrin $\alpha_v\beta_3$-specificity, each animal was administered with ~2

μCi of ^{99m}TcO(MAG$_2$-3P-RGD$_2$) along with ~350 μg of E[c(RGDfK)]$_2$ (~14 mg/kg). At 1 h p.i., five animals were sacrificed by sodium pentobarbital overdose (100 mg/kg) for organ biodistribution. The organ uptake (%ID/g) was compared to that obtained in the absence of excess E[c(RGDfK)]$_2$ at the same time point. For the experiment to demonstrate the radiotracer RGD-specific, each animal was administered with ~2 μCi of ^{99m}TcO(MAG$_2$-3P-RGD$_2$) along with ~350 μg of E[c(RGDfK)]$_2$ (~14 mg/kg). At 1 h p.i., five animals were sacrificed by sodium pentobarbital overdose (100 mg/kg) for organ biodistribution. The organ uptake (%ID/g) was compared to that obtained in the absence of excess E[c(RGDfK)]$_2$ at the same time point.

Scintigraphic Imaging

Three athymic nude mice bearing U87MG glioma xenografts were used for planar imaging studies. Each glioma-bearing mouse was intravenously administered with ~500 μCi of ^{99m}TcO(MAG$_2$-3P-RGD$_2$) via tail vein. The animals were anesthetized with intramuscular injection of ketamine (80 mg/kg) and xylazine (19 mg/kg). The animal was placed prone on a single head mini γ-camera (Diagnostic Services Inc., NJ) equipped with a parallel-hole, low-energy, and high-resolution collimator. Static images were acquired at 15, 30, 60 and 120 min p.i. and were stored digitally in a 128×128 matrix. The acquisition count limits were set at 500 K. After imaging, the animals were euthanized by sodium pentobarbital overdose (100 – 200 mg/kg).

Metabolism

Three glioma-bearing mice were used for the in vivo metabolic stability study of ^{99m}TcO(MAG$_2$-3P-RGD$_2$), which was intravenously administered at the dose of ~100 μCi per mouse via tail vein. At 120 min p.i., the urine samples were collected, and were mixed with equal volume of 20% acetonitrile aqueous solution. The mixture was centrifuged at 8,000 rpm for 5 min. The supernatant was collected and filtered through a 0.20 μ Millex-LG filter unit. The feces samples were collected at 120 min p.i. and suspended in a mixture of 20% acetonitrile aqueous solution (2 mL). The resulting mixture was vortexed for 10 min. After centrifuging at 8,000 rpm for 5 min, the supernatant was collected and passed through a 0.20 μ Millex-LG filter unit to remove any particles or precipitate. Both the urine and feces samples were analyzed by radio-HPLC (Method 2). The tumor, kidney, and liver tissues were harvested at 120 min p.i. counted in a Perkin Elmer Wizard – 1480 γ-counter (Shelton, CT) for total radioactivity, and was then homogenized. The homogenate was mixed with 2 mL of 20% acetonitrile aqueous solution. After centrifuging at 8,000 rpm for 5 min, the supernatant was collected and counted on a γ-counter to determine the percentage of radioactivity recovery in each organ. After filtration through a 0.20 μm Millex-LG filter unit to remove foreign particles or precipitate, the filtrate was then analyzed by radio-HPLC (Method 2).

Data and Statistical Analysis

The biodistribution data and target-to-background (T/B) ratios are reported as an average plus the standard variation based on results from four tumor-bearing mice at each time point. Comparison between two different ^{99m}Tc radiotracers was made using the two-way ANOVA test (GraphPad Prim 5.0, San Diego, CA). The level of significance was set at $p < 0.05$.

Results

MAG_2 Conjugate Synthesis

Synthesis of new cyclic RGD peptide conjugates (MAG_2-P-RGD_2 and MAG_2-3P-RGD_2) was straightforward. They were prepared by conjugation of P-RGD_2 and 3P-RGD_2, respectively, with excess MAG_2-NHS in DMF in the presence of a base, such as DIEA. MAG_2-3P-RGK_2 contains two c(RGKfD) motifs instead of c(RGDfK) motifs in MAG_2-3P-RGD_2, and was prepared as a "negative control" to demonstrate the RGD-specificity of ^{99m}TcO(MAG_2-3P-RGD_2). All new peptide conjugates were purified twice by HPLC (Method 1), and characterized by ESI-MS. Their HPLC purity was >95% before being used for ^{99m}Tc-labeling and determination of their integrin $\alpha_v\beta_3$ binding affinity.

Integrin $\alpha_v\beta_3$ Binding Affinity

The integrin $\alpha_v\beta_3$ binding affinity of c(RGDfK), MAG_2-3P-RGD_2 and MAG_2-3P-RGD_2 and MAG_2-3P-RGK_2 were determined by a competitive displacement assay. Their IC_{50} values were obtained from curve fitting from Figure 2, and were calculated to be 46.6 ± 4.5, 8.6 ± 2.8, 3.9 ± 0.4 and 711 ± 128 nM, respectively.

Radiochemistry

^{99m}TcO(MAG_2-P-RGD_2) and ^{99m}TcO(MAG_2-3P-RGD_2) were prepared by reacting MAG_2-P-RGD_2 and MAG_2-3P-RGD_2, respectively, with $^{99m}TcO_4^-$ at pH ~8.5 in the presence of excess D-glucoheptonic acid (~50 mg per vial) and stannous chloride. ^{99m}Tc-labeling was accomplished by heating the reaction mixture at 100 °C for 15 – 20 min. D-glucoheptonic acid was used to stabilize $SnCl_2$ and the $[^{99m}TcO]^{3+}$ core, and to prevent formation of [^{99m}Tc]colloid during radiolabeling. Their radiochemical purity was >90% with <0.5% of [^{99m}Tc]colloid. In general, 20 – 25 μg MAG_2-3P-RGD_2 was sufficient for successful radiolabeling of 50 mCi of $^{99m}TcO_4^-$. The specific activity for ^{99m}TcO(MAG_2-3P-RGD_2) was ~2.0 mCi/μg (~5 Ci/μmol). ^{99m}TcO(MAG_2-3P-RGD_2) was stable in the kit matrix for >6 h. All ^{99m}Tc radiotracers were analyzed by the same HPLC method, and their retention times were listed in Table 1. The log P values for ^{99m}TcO(MAG_2-P-RGD_2), ^{99m}TcO(MAG_2-3P-RGD_2) and ^{99m}TcO(MAG_2-3P-RGK_2) were determined to be -3.30 ± 0.13, -3.19 ± 0.10 and -2.40 ± 0.14, respectively.

Biodistribution Characteristics

The biodistribution data for ^{99m}TcO(MAG_2-P-RGD_2) and ^{99m}TcO(MAG_2-3P-RGD_2) were listed in Tables 2 and 3, respectively. ^{99m}TcO(MAG_2-P-RGD_2) had the tumor uptake of 10.41 ± 2.07 and 11.56 ± 1.41 %ID/g at 30 and 60 min, respectively, but it decreased to 5.66 ± 0.50 %ID/g at 120 min p.i. It also had a high kidney uptake with a fast clearance (19.01 ± 1.48 and 4.02 ± 0.81 % ID/g at 30 and 120 min p.i., respectively). The liver uptake of ^{99m}TcO(MAG_2-P-RGD_2) was 4.84 ± 0.87, 3.11 ± 0.30 and 1.43 ± 0.20 %ID/g while its tumor/liver ratios were 2.34 ± 0.58, 3.78 ± 0.27 and 3.99 ± 0.52 at 30, 60 and 120 min p.i., respectively. ^{99m}TcO(MAG_2-3P-RGD_2) also had a high tumor uptake (16.78 ± 5.46, 15.48 ± 2.49 and 13.60 ± 2.30 %ID/g at 30, 60 and 120 min p.i., respectively). Its kidney uptake was 18.68 ± 2.10, 13.38 ± 2.07 and 6.43 ± 0.89 % ID/g at 30, 60 and 120 min p.i. respectively. Its liver uptake was 4.97 ± 0.68 %ID/g at 30 min p.i. and 2.38 ± 0.17 %ID/g at 120 min p.i., and its tumor/liver ratio increased steadily from 3.39 ± 1.03 at 30 min p.i. to 5.71 ± 0.82 at 120 min p.i.

Effects of Technetium Chelate

To assess the impact of ^{99m}Tc chelates (^{99m}TcO(MAG_2) vs. [^{99m}Tc(HYNIC)(tricine)(TPPTS)]) on the radiotracer tumor uptake and T/B ratios, we also obtained the 60-min

biodistribution data of ^{99m}Tc-3P-RGD$_2$ using the same animal model with similar tumor size. Figure 4 compares the organ uptake and T/B ratios for ^{99m}TcO(MAG$_2$-3P-RGD$_2$) and ^{99m}Tc-3P-RGD$_2$ at 60 min p.i. Replacing [^{99m}Tc(HYNIC)(tricine)(TPPTS)] with the much smaller ^{99m}TcO(MAG$_2$) resulted in a significant increase in the tumor and normal organ uptake. For example, ^{99m}TcO(MAG$_2$-3P-RGD$_2$) had the 60-min uptake of 15.48 ± 2.49, 1.40 ± 0.67, 9.39 ± 1.69, 13.38 ± 2.07, 3.87 ± 0.51 and 5.29 ± 0.79 %ID/g in the tumor, blood, intestine, kidneys, liver and lungs, respectively, while the uptake of ^{99m}Tc-3P-RGD$_2$ in the same organs was 9.15 ± 2.13, 0.27 ± 0.08, 5.25 ± 1.92, 8.22 ± 1.99, 1.69 ± 0.46 and 2.10 ± 0.54 %ID/g at the same time point.

Integrin $\alpha_v\beta_3$ Specificity

Figure 6A compares the organ uptake of ^{99m}TcO(MAG$_2$-3P-RGD$_2$) in the absence/presence of E[c(RGDfK)]$_2$ at 60 min p.i. Co-injection of excess E[c(RGDfK)]$_2$ almost completely blocked its tumor uptake (0.31 ± 0.07 %ID/g with E[c(RGDfK)]$_2$ vs. 15.48 ± 2.49 %ID/g without E[c(RGDfK)]$_2$). The normal organ uptake of ^{99m}TcO(MAG$_2$-3P-RGD$_2$) was also almost completely blocked by co-injection of excess E[c(RGDfK)]$_2$.

RGD Specificity

Figure 6B compares the 60-min organ uptake values for ^{99m}TcO(MAG$_2$-3P-RGK$_2$) and ^{99m}TcO(MAG$_2$-3P-RGD$_2$). This experiment was designed to demonstrate the RGD-specificity of ^{99m}TcO(MAG$_2$-3P-RGD$_2$). ^{99m}TcO(MAG$_2$-3P-RGK$_2$) had much lower tumor uptake (0.70 ± 0.09 %ID/g) than ^{99m}TcO(MAG$_2$-3P-RGD$_2$) (15.48 ± 2.49 %ID/g). It also had significantly ($p < 0.01$) lower uptake in normal organs than ^{99m}TcO(MAG$_2$-3P-RGD$_2$). As a result, the radioactivity was excreted much faster (more urine activity at the same time point) from the renal route in the tumor-bearing mice administered with ^{99m}TcO(MAG$_2$-3P-RGK$_2$).

Tumor Size vs. Tumor Uptake

In this study, we used a total of 14 glioma-bearing mice to explore the relationship between the tumor size and %ID uptake of ^{99m}TcO(MAG$_2$-3P-RGD$_2$) at 120 min p.i. As illustrated in Figure 5A, there was a linear relationship between the tumor size (0.08 – 0.4 g; n = 14) and the %ID glioma uptake of ^{99m}TcO(MAG$_2$-3P-RGD$_2$) with $R^2 = 0.9226$. Obviously, the %ID tumor uptake of ^{99m}TcO(MAG$_2$-3P-RGD$_2$) increased in a linear fashion as the tumor size became larger.

Planar Imaging

Figure 7 illustrates representative static images of the glioma-bearing mice (n = 3) administered with ^{99m}TcO(MAG$_2$-3P-RGD$_2$) at 15, 30, 60 and 120 min p.i. The tumor was clearly seen with excellent contrast as early as 15 min p.i. The tumor radioactivity remained relatively steady over the 2 h study period. The radioactivity accumulation in the blood and muscle disappeared almost completely by 120 min p.i. The most visible organs were tumor, gallbladder, kidneys and bladder. Because of the radioactivity accumulation in the abdominal region, it was difficult to accurately determine the tumor/kidney and tumor/liver ratios on the basis of planar imaging.

Metabolic Properties

Metabolism studies were performed on ^{99m}TcO(MAG$_2$-3P-RGD$_2$) using athymic nude mice bearing U87MG glioma xenografts. The percentage of radioactivity recovery in the urine and feces samples was very high (>90%); but it was only 45 – 55% from the homogenates of the tumor, kidney and liver tissues. Figure 8 shows radio-HPLC chromatograms of ^{99m}TcO(MAG$_2$-3P-RGD$_2$) in saline before injection, in the extracts of urine and feces

samples, and in the homogenates from tumor, kidneys, and liver at 120 min p.i. There was no significant metabolism for ^{99m}TcO(MAG$_2$-3P-RGD$_2$) during its excretion from renal and hepatobiliary routes, and in the tissues from tumor, liver and kidneys.

Discussion

In this study, we prepared two cyclic RGD dimer conjugates (MAG$_2$-P-RGD$_2$and MAG$_2$-3P-RGD$_2$). It is found that both ^{99m}TcO(MAG$_2$-P-RGD$_2$) and ^{99m}TcO(MAG$_2$-3P-RGD$_2$), can be obtained in high yield (>90%) and with high specific activity (~5 Ci/μmol) using a kit formulation, and have very high solution stability in the kit matrix. There are advantages of using small peptides, such as MAG$_2$ (the smallest N_3S triamidethiol chelating unit when conjugated to the peptide) as BFCs. The attachment of BFC can be easily incorporated into solid-phase peptide synthesis. The N_3S chelating units form stable Tc complexes with the $[Tc=O]^{3+}$ core. The hydrophilicity of the Tc chelate can be tuned by changing the glycine residues with more hydrophilic amino acids, such as aspartic and glutamic acids.

The integrin $\alpha_v\beta_3$ binding affinity follows the order of MAG$_2$-3P-RGD$_2$ (IC_{50} = 3.9 ± 0.4 nM) > MAG$_2$-P-RGD$_2$ (IC_{50} = 8.6 ± 2.8 nM) > c(RGDfK) (IC_{50} = 46.6 ± 4.5 nM), suggesting that bivalency is most likely responsible for the higher integrin $\alpha_v\beta_3$ binding affinity of MAG$_2$-3P-RGD$_2$ as compared to that of MAG$_2$-P-RGD$_2$. This conclusion is well supported by the significantly ($p < 0.01$) higher tumor uptake (Figure 3) of ^{99m}TcO(MAG$_2$-3P-RGD$_2$) than that of ^{99m}TcO(MAG$_2$-P-RGD$_2$). If they were bound to integrin $\alpha_v\beta_3$ in the same fashion, MAG$_2$-3P-RGD$_2$ and MAG$_2$-P-RGD$_2$ would have had the same integrin $\alpha_v\beta_3$ binding affinity whereas ^{99m}TcO(MAG$_2$-3P-RGD$_2$) and ^{99m}TcO(MAG$_2$-P-RGD$_2$) would have shared the similar tumor uptake in the same tumor-bearing animal model.

The integrin $\alpha_v\beta_3$ binding affinity of MAG$_2$-3P-RGD$_2$ (IC_{50} = 3.9 ± 0.4 nM) is very similar to that of HYNIC-3P-RGD$_2$ (IC_{50} = 4.1 ± 0.3 nM), respectively, suggesting that replacing HYNIC with MAG$_2$ has little impact on the integrin $\alpha_v\beta_3$ binding affinity of 3P-RGD$_2$. It must be noted that this comparison is between the cyclic RGD conjugates, not their ^{99m}Tc radiotracers, the integrin $\alpha_v\beta_3$ binding affinity and biodistribution characteristic of which could be altered significantly depending on the size of ^{99m}Tc chelates (Figure 1: ^{99m}TcO(MAG$_2$) vs. [^{99m}Tc(HYNIC)(tricine)(TPPTS)]). ^{99m}TcO(MAG$_2$) has a molecular weight of ~300 Daltons, and is expected to have minimal impact on integrin $\alpha_v\beta_3$ binding affinity of 3PEG$_4$-dimer. In contrast, [^{99m}Tc(HYNIC)(tricine)(TPPTS)] has a molecular weight of ~1000 Daltons due to the presence of tricine and TPPTS coligands, and is expected to have much more significant impact on the integrin $\alpha_v\beta_3$ binding affinity of 3P-RGD$_2$. This assumption seems to be supported by the significantly ($p < 0.01$) higher tumor uptake of ^{99m}TcO(MAG$_2$-3P-RGD$_2$) (15.48 ± 2.49 %ID/g at 60 min p.i.) than that of ^{99m}Tc-3P-RGD$_2$ (9.15 ± 2.13 at 60 min p.i.).

Replacing [^{99m}Tc(HYNIC)(tricine)(TPPTS)] with ^{99m}TcO(MAG$_2$) results in >10× higher lipophilicity for ^{99m}TcO(MAG$_2$-3P-RGD$_2$) (log P = -3.19 ± 0.13) as compare to ^{99m}Tc-3P-RGD$_2$ (log P = -4.35 ± 0.10), which is most likely responsible for its higher uptake in tumor, blood and normal organs (Figure 4: top). For example, the blood radioactivity for ^{99m}TcO(MAG$_2$-3P-RGD$_2$) is 1.40 ± 0.67 %ID/g at 60 min p.i. while it is only 0.27 ± 0.08 %ID/g for ^{99m}Tc-3P-RGD$_2$ at the same time point. The liver uptake of ^{99m}TcO(MAG$_2$-3P-RGD$_2$) is 3.87 ± 0.51 %ID/g whereas ^{99m}Tc-3P-RGD$_2$ has the liver uptake of 2.92 ± 0.77 %ID/g at 60 min p.i. ^{99m}TcO(MAG$_2$-3P-RGD$_2$) has the kidney uptake of 13.38 ± 2.07 %ID/g while ^{99}Tc-3PEG$_4$-dimer has the kidney uptake of 8.62 ± 1.99 %ID/g at 60 min p.i. The lung uptake is 5.29 ± 0.79 %ID/g for ^{99m}TcO(MAG$_2$-3P-RGD$_2$) and 2.10

± 0.54 %ID/g for ^{99m}Tc-3P-RGD$_2$ at 60 min p.i. As a result, the tumor/blood, tumor/liver, tumor/lung and tumor/liver ratios for ^{99m}TcO(MAG$_2$-3P-RGD$_2$) are not as good as those for ^{99m}Tc-3P-RGD$_2$ (Figure 4: bottom). On the basis of these data, we believe that ^{99m}Tc-3P-RGD$_2$ remains to be a better SPECT radiotracer for noninvasive imaging of integrin $\alpha_v\beta_3$–positive tumors.

The integrin $\alpha_v\beta_3$-specificity of ^{99m}TcO(MAG$_2$-3P-RGD$_2$) has been demonstrated by the "blocking experiment" (Figure 6A). The blockage of its tumor uptake indicates that ^{99m}TcO(MAG$_2$-3P-RGD$_2$) is integrin $\alpha_v\beta_3$-specific. The uptake blockage in the eyes, heart, intestine, lungs, liver and spleen suggests that its accumulation in these organs is also integrin $\alpha_v\beta_3$-mediated. This conclusion is supported by the immunohistopathological studies (34, 35), which showed a strong positive staining of endothelial cells of small glomeruli vessels in the kidneys and weak staining in branches of the hepatic portal vein. The RGD-specificity of ^{99m}TcO(MAG$_2$-3P-RGD$_2$) is demonstrated by the lower integrin $\alpha_v\beta_3$ binding affinity of MAG$_2$-3P-RGK$_2$ (IC_{50} = 711 ± 128 nM) than that of MAG$_2$-3P-RGD$_2$ (IC_{50} = 3.9 ± 0.4 nM), and the lower tumor uptake of ^{99m}TcO(MAG$_2$-3P-RGK$_2$) than that of ^{99m}TcO(MAG$_2$-3P-RGD$_2$) (Figure 6B). In addition, ^{99m}TcO(MAG$_2$-3PEG$_4$-dimer) is able to maintain its chemical integrity during excretion from both renal and hepatobiliary routes, and in the tumor and liver tissues (Figure 8).

The ability to non-invasively quantify the integrin $\alpha_v\beta_3$ level provides new opportunities to select appropriate patients for anti-angiogenic treatment of integrin $\alpha_v\beta_3$-positive cancer patients (59,60). The %ID tumor uptake reflects the total integrin $\alpha_v\beta_3$ level while the %ID/g tumor uptake reflects the integrin $\alpha_v\beta_3$ density. When tumor is small (<0.05 g or 50 m^3), there is little angiogenesis with low blood flow. As a result, ^{99m}TcO(MAG$_2$-3P-RGD$_2$) has low %ID tumor uptake (Figure 5A). As tumor grows, the integrin $\alpha_v\beta_3$ level becomes higher, and the %ID tumor uptake of ^{99m}TcO(MAG$_2$-3P-RGD$_2$) increases (Figure 5A). The linear relationship between the tumor size and %ID tumor uptake strongly suggests that ^{99m}TcO(MAG$_2$-3P-RGD$_2$) has the potential for monitoring the integrin $\alpha_v\beta_3$ expression levels during anti-angiogenic therapy. It is important to note that the integrin $\alpha_v\beta_3$ expression is not homogenous in the tumor tissue. Parts of the tumor tissue may become necrotic when its size is >10 mm in diameter. Therefore, the radiotracer %ID/g uptake in the tumors of different size is scattered as previously reported for ^{99m}Tc-3P-RGD$_2$ (55), ^{99m}Tc-3G-RGD$_2$ (56), and ^{64}Cu(DOTA-3P-RGD$_2$) (57).

We must be concerned that the subcutaneous glioma-bearing model used in this study may not reflect the real tumor growth rate in glioma cancer patients since the tumor growth is too fast in the athymic nude mice bearing U87MG glioma xenografts. However, this tumor-bearing animal model as a screening tool should provide us sufficient biodistribution data to select an optimal radiotracer for more preclinical evaluations in the future. In addition, we also noticed that the tumor growth rate is largely dependent on the number of U87MG human glioma cells implanted in each animal, and the radiotracer tumor uptake may vary significantly with the tumor growth rate. Whenever possible, the comparison between different radiotracers should be made by using their biodistribution data obtained from the same groups of tumor-bearing mice with similar tumor size. That is why in this study we obtained the 60-min biodistribution data of ^{99m}Tc-3PEG$_4$-dimer, instead of using those reported in our previous studies (55), to demonstrate the impact of ^{99m}Tc chelates (^{99m}TcO(MAG$_2$) vs. [^{99m}Tc(HYNIC)(tricine)(TPPTS)]) on radiotracer tumor uptake and T/B ratios.

Conclusion

In this study, we presented the synthesis of two cyclic RGD peptide conjugates, MAG_2-P-RGD_2 and MAG_2-3P-RGD_2, and evaluated $^{99m}TcO(MAG_2\text{-P-}RGD_2)$ and $^{99m}TcO(MAG_2\text{-3P-}RGD_2)$ as new radiotracers for noninvasive imaging of integrin $\alpha_v\beta_3$ expression in athymic nude mice bearing U87MG glioma xenografts. The key findings are: (1) MAG_2 is such an efficient BFC that $^{99m}TcO(MAG_2\text{-3P-}RGD_2)$ could be readily prepared in high yield with high specific activity using a single-vial kit formulation; (2) replacing [^{99m}Tc(HYNIC)(tricine)(TPPTS)] with $^{99m}TcO(MAG_2)$ results in a significant increase in the radiotracer uptake in the tumor, blood and normal organs due to the increased lipophilicity of $^{99m}TcO(MAG_2\text{-3P-}RGD_2)$. Even though $^{99m}TcO(MAG_2\text{-3P-}RGD_2)$ has the better tumor uptake, its tumor/blood, tumor/liver, tumor/lung and tumor/liver ratios are not as good as those for ^{99m}Tc-3P-RGD_2. On the basis of these results, we believe that future research should be directed towards BFC with highly charged amino acid residues, such as aspartic and glutamic acids, instead of glycine in MAG_2.

Acknowledgments

This work is supported, in part, by Purdue University and research grants: R01 CA115883 A2 (S.L.) from National Cancer Institute (NCI), R21 HL083961-01 (S.L.) from the National Heart, Lung, and Blood Institute (NHLBI), and DE-FG02-08ER64684 (S.L.) from the Department of Energy, and NSF-30780728 (F.W.) from the National Science Foundation of China.

References

1. Weber WA, Haubner R, Vabuliene E, Kuhnast B, Webster HJ, Schwaiger M. Tumor angiogenesis targeting using imaging agents. Q J Nucl Med 2001;45:179–182. [PubMed: 11476168]
2. Liu S, Edwards DS. Fundamentals of receptor-based diagnostic metalloradiopharmaceuticals. Topics in Current Chem 2002;222:259–278.
3. Van de Wiele C, Oltenfreiter R, De Winter O, Signore A, Slegers G, Dieckx RA. Tumor angiogenesis pathways: related clinical issues and implications for nuclear medicine imaging. Eur J Nucl Med 2002;29:699–709.
4. Liu S, Robinson SP, Edwards DS. Integrin $\alpha_v\beta_3$ directed radiopharmaceuticals for tumor imaging. Drugs of the Future 2003;28:551–564.
5. Haubner R, Wester HJ. Radiolabeled tracers for imaging of tumor angiogenesis and evaluation of antiantiogenic therapies. Current Pharmaceutical Design 2004;10:1439–1455. [PubMed: 15134568]
6. D'Andrea LD, Del Gatto A, Pedone C, Benedetti E. Peptide-based molecules in angiogenesis. Chem Biol Drug Des 2006;67:115–126. [PubMed: 16492159]
7. Meyer A, Auremheimer J, Modlinger A, Kessler H. Targeting RGD recognizing integrins: drug development, biomaterial research, tumor imaging and targeting. Current Pharmaceutical Design 2006;12:2723–2747. [PubMed: 16918408]
8. Chen X. Multimodality imaging of tumor integrin $\alpha_v\beta_3$ expression. Mini-Rev Med Chem 2006;6:227–234. [PubMed: 16472190]
9. Liu S. Radiolabeled multimeric cyclic RGD peptides as integrin $\alpha_v\beta_3$-targeted radiotracers for tumor imaging. Mol Pharm 2006;3:472–487. [PubMed: 17009846]
10. Cai W, Chen X. Multimodality molecular imaging of tumor angiogenesis. J Nucl Med 2008;49:113S–128S. [PubMed: 18523069]
11. Cai W, Niu G, Chen X. Imaging of integrins as biomarkers for tumor angiogenesis. Current Pharmaceutical Design 2008;14:2943–2973. [PubMed: 18991712]
12. Hsu A, Chen X. Advances in anatomic, functional, and molecular imaging of angiogenesis. J Nucl Med 2008;49:511–514. [PubMed: 18375921]
13. Van Hagen PM, Breeman WAP, Bernard HF, Schaar M, Mooij CM, Srinivasan A, Schmidt MA, Krenning EP, de Jong M. Evaluation of a radiolabeled cyclic DTPA-RGD analog for tumor imaging and radionuclide therapy. Int J Cancer (Radiat Oncol Invest) 2000;90:186–198.

14. Huabner R, Wester HJ, Senekowitsch-Schmidtke R, Diefenbach B, Kessler H, Stöcklin G, Schwaiger M. RGD-peptides for tumor targeting: biological evaluation of radioiodinated analogs and introduction of a novel glycosylated peptide with improved biokinetics. J Labelled Compounds & Radiopharmaceuticals 1997;40:383–385.
15. Sivolapenko GB, Skarlos D, Pectasides D, Stathopoulou E, Milonakis A, Sirmalis G, Stuttle A, Courtenay-Luck NS, Konstantinides K, Epenetos AA. Imaging of metastatic melanoma utilizing a technetium-99m labeled RGD-containing synthetic peptide. Eur J Nucl Med 1998;25:1383–1389. [PubMed: 9818277]
16. Haubner R, Wester HJ, Weber WA, Mang C, Ziegler SI, Goodman SL, Senekowisch-Schmidtke R, Kessler H, Schwaiger M. Noninvasive imaging of $\alpha_v\beta_3$ integrin expression using ^{18}F-labeled RGD-containing glycopeptide and positron emission tomography. Cancer Res 2001;61:1781–1785. [PubMed: 11280722]
17. Haubner R, Wester HJ, Reuning U, Senekowisch-Schmidtke R, Diefenbach B, Kessler H, Stöcklin G, Schwaiger M. Radiolabeled $\alpha_v\beta_3$ integrin antagonists: a new class of tracers for tumor imaging. J Nucl Med 1999;40:1061–1071. [PubMed: 10452325]
18. Haubner R, Wester HJ, Burkhart F, Senekowisch-Schmidtke R, Weber W, Goodman SL, Kessler H, Schwaiger M. Glycolated RGD-containing peptides: tracer for tumor targeting and angiogenesis imaging with improved biokinetics. J Nucl Med 2001;42:326–336. [PubMed: 11216533]
19. Haubner R, Bruchertseifer F, Bock M, Schwaiger M, Wester HJ. Synthesis and biological evaluation of ^{99m}Tc-labeled cyclic RGD peptide for imaging the $\alpha_v\beta_3$ expression. Nuklearmedizin 2004;43:26–32. [PubMed: 14978538]
20. Thumshirn G, Hersel U, Goodman SL, Kessler H. Multimeric cyclic RGD peptides as potential tools for tumor targeting: solid-phase peptide synthesis and chemoselective oxime ligation. Chem Eur J 2003;9:2717–2725.
21. Poethko T, Schottelius M, Thumshirn G, Herz M, Haubner R, Henriksen G, Kessler H, Schwaiger M, Wester HJ. Chemoselective pre-conjugate radiohalogenation of unprotected mono- and multimeric peptides via oxime formation. Radiochim Acta 2004;92:317–327.
22. Poethko T, Schottelius M, Thumshirn G, Hersel U, Herz M, Henriksen G, Kessler H, Schwaiger M, Wester HJ. Two-step methodology for high yield routine radiohalogenation of peptides: ^{18}F-labeled RGD and octreotide analogs. J Nucl Med 2004;45:892–902. [PubMed: 15136641]
23. Alves S, Correia JDG, Gano L, Rold TL, Prasanphanich A, Haubner R, Rupprich M, Alberto R, Decristoforo C, Snatos I, Smith CJ. In vitro and in vivo evaluation of a novel ^{99m}Tc(CO)$_3$-pyrazolyl conjugate of *cyclo*-(Arg-Gly-Asp-D-Tyr-Lys). Bioconj Chem 2007;18:530–537.
24. Fani M, Psimadas D, Zikos C, Xanthopoulos S, Loudos GK, Bouziotis P, Varvarigou AD. Comparative evaluation of linear and cyclic ^{99m}Tc-RGD peptides for targeting of integrins in tumor angiogenesis. Anticancer Res 2006;26:431–434. [PubMed: 16475729]
25. Su ZF, Liu G, Gupta S, Zhu Z, Rusckowski M, Hnatowich DJ. In vitro and in vivo evaluation of a technetium-99m-labeled cyclic RGD peptide as specific marker of $\alpha_v\beta_3$ integrin for tumor imaging. Bioconj Chem 2002;13:561–570.
26. Decristoforo C, Faintuch-Linkowski B, Rey A, vo Guggenberg E, Rupprich M, Hernandez-Gonzales I, Rodrigo T, Haubner R. [^{99m}Tc]HYNIC-RGD for imaging integrin $\alpha_v\beta_3$ expression. Nucl Med Biol 2006;33:945–952. [PubMed: 17127166]
27. Chen X, Park R, Tohme M, Shahinian AH, Bading JR, Conti PS. MicroPET and autoradiographic imaging of breast cancer α_v-integrin expression using ^{18}F- and ^{64}Cu-labeled RGD peptide. Bioconj Chem 2004;15:41–49.
28. Chen X, Park R, Shahinian AH, Tohme M, Khankaldyyan V, Bozorgzadeh MH, Bading JR, Moats R, Laug WE, Conti PS. ^{18}F-labeled RGD peptide: initial evaluation for imaging brain tumor angiogenesis. Nucl Med Bio 2004;31:179–189. [PubMed: 15013483]
29. Chen X, Park R, Shahinian AH, Bading JR, Conti PS. Pharmacokinetics and tumor retention of ^{125}I-labeled RGD peptide are improved by PEGylation. Nucl Med Biol 2004;31:11–19. [PubMed: 14741566]

30. Chen X, Liu S, Hou Y, Tohme M, Park R, Bading JR, Conti PS. MicroPET imaging of breast cancer α_v-integrin expression with ^{64}Cu-labeled dimeric RGD peptides. Mol Imag Biol 2004;6:350–359.

31. Chen X, Tohme M, Park R, Hou Y, Bading JR, Conti PS. MicroPET imaging of breast cancer α_v-integrin expression with ^{18}F-labeled dimeric RGD peptide. Mol Imaging 2004;3:96–104. [PubMed: 15296674]

32. Wu Y, Zhang X, Xiong Z, Cheng Z, Fisher DR, Liu S, Gambhir SS, Chen X. MicroPET imaging of glioma integrin $\alpha_v\beta_3$ expression using ^{64}Cu-labeled tetrameric RGD peptide. J Nucl Med 2005;46:1707–1718. [PubMed: 16204722]

33. Zhang X, Xiong Z, Wu Y, Cai W, Tseng JR, Gambhir SS, Chen X. Quantitative PET imaging of tumor integrin $\alpha_v\beta_3$ expression with ^{18}F-FRGD2. J Nucl Med 2006;47:113–121. [PubMed: 16391195]

34. Wu Z, Li Z, Chen K, Cai W, He L, Chin FT, Li F, Chen X. Micro-PET of tumor integrin $\alpha_v\beta_3$ expression using ^{18}F-labeled PEGylated tetrameric RGD peptide (^{18}F-FPRGD4). J Nucl Med 2007;48:1536–1544. [PubMed: 17704249]

35. Zhang X, Chen X. Preparation and characterization of ^{99m}Tc(CO)$_3$-BPy-RGD complex as $\alpha_v\beta_3$ integrin receptor-targeted imaging agent. Appl Radiat Isotopes 2007;65:70–78.

36. Li ZB, Chen K, Chen X. ^{68}Ga-labeled multimeric RGD peptides for microPET imaging of integrin $\alpha_v\beta_3$ expression. Eur J Nucl Med Mol Imaging 2008;35:1100–1108. [PubMed: 18204838]

37. Liu S, Cheung E, Rajopadyhe M, Ziegler MC, Edwards DS. ^{90}Y- and ^{177}Lu-labeling of a DOTA-conjugated vitronectin receptor antagonist for tumor therapy. Bioconj Chem 2001;12:559–568.

38. Janssen M, Oyen WJG, Massuger LFAG, Frielink C, Dijkgraaf I, Edwards DS, Rajopadyhe M, Corsten FHM, Boerman OC. Comparison of a monomeric and dimeric radiolabeled RGD-peptide for tumor targeting. Cancer Biother Radiopharm 2002;17:641–646. [PubMed: 12537667]

39. Janssen M, Oyen WJG, Dijkgraaf I, Massuger LFAG, Frielink C, Edwards DS, Rajopadyhe M, Boonstra H, Corsten FHM, Boerman OC. Tumor targeting with radiolabeled integrin $\alpha_v\beta_3$ binding peptides in a nude mice model. Cancer Res 2002;62:6146–6151. [PubMed: 12414640]

40. Janssen ML, Frielink C, Dijkgraaf I, Oyen WJ, Edwards DS, Liu S, Rajopadhye M, Massuger LF, Corstens FHM, Boerman OC. Improved tumor targeting of radiolabeled RGD-peptides using rapid dose fractionation. Cancer Biother Radiopharm 2004;19:399–404. [PubMed: 15453954]

41. Liu S, Hsieh WY, Kim YS, Mohammed SI. Effect of coligands on biodistribution characteristics of ternary ligand ^{99m}Tc complexes of a HYNIC-conjugated cyclic RGDfK dimer. Bioconj Chem 2005;16:1580–1588.

42. Jia B, Shi J, Yang Z, Xu B, Liu Z, Zhao H, Liu S, Wang F. ^{99m}Tc-labeled cyclic RGDfK dimer: initial evaluation for SPECT imaging of glioma integrin $\alpha_v\beta_3$ expression. Bioconj Chem 2006;17:1069–1076.

43. Liu S, He ZJ, Hsieh WY, Kim YS, Jiang Y. Impact of PKM linkers on biodistribution characteristics of the ^{99m}Tc-labeled cyclic RGDfK dimer. Bioconj Chem 2006;17:1499–1507.

44. Liu S, Hsieh WY, Jiang Y, Kim YS, Sreerama SG, Chen X, Jia B, Wang F. Evaluation of a ^{99m}Tc-labeled cyclic RGD tetramer for noninvasive imaging integrin $\alpha_v\beta_3$-positive breast cancer. Bioconj Chem 2007;18:438–446.

45. Dijkgraaf I, Liu S, Kruijtzer JAW, Soede AC, Oyen WJG, Liskamp RMJ, Corstens FHM, Boerman OC. Effects of linker variation on the in vitro and in vivo characteristics of an ^{111}In-labeled RGD Peptide. Nucl Med Biol 2007;34:29–35. [PubMed: 17210459]

46. Dijkgraaf I, John AW, Kruijtzer JAW, Liu S, Soede A, Oyen WJG, Corstens FHM, Liskamp RMJ, Boerman OC. Improved targeting of the $\alpha_v\beta_3$ integrin by multimerization of RGD peptides. Eur J Nucl Med Mol Imaging 2007;34:267–273. [PubMed: 16909226]

47. Liu S, Kim YS, Hsieh WY, Sreerama SG. Coligand effects on solution stability, biodistribution and metabolism of ^{99m}Tc-labeled cyclic RGDfK tetramer. Nucl Med Biol 2008;35:111–121. [PubMed: 18158950]

48. Jia B, Liu Z, Shi J, Yu ZL, Yang Z, Zhao HY, He ZJ, Liu S, Wang F. Linker effects on biological properties of ^{111}In-labeled DTPA conjugates of a cyclic RGDfK dimer. Bioconj Chem 2008;19:201–210.

49. Wang JJ, Kim YS, Liu S. ^{99m}Tc-labeling of HYNIC-conjugated cyclic RGDfK dimer and tetramer using EDDA as coligand. Bioconj Chem 2008;19:634–642.
50. Morrison MS, Ricketts SA, Barnett J, Cuthbertson A, Jean Tessier J, Wedge SR. Use of a novel Arg-Gly-Asp radioligand, ^{18}F-AH111585, to determine changes in tumor vascularity after antitumor therapy. J Nucl Med 2009;50:116–122. [PubMed: 19091899]
51. Kenny LM, Coombes RC, Oulie I, Contractor KB, Miller M, Spinks TJ, McParland B, Cohen PS, Hui A, Palmieri C, Osman S, Glaser M, Turton D, Al-Nahhas A, Anoagye EO. Phase I trial of the positron-emitting Arg-Gly-Asp (RGD) peptide radioligand ^{18}F-AH111585 in breast cancer patients. J Nucl Med 2008;49:879–886. [PubMed: 18483090]
52. Beer AJ, Haubner R, Goebel M, Luderschmidt S, Spilker ME, Webster HJ, Weber WA, Schwaiger M. Biodistribution and pharmacokinetics of the $\alpha_v\beta_3$-selective tracer ^{18}F-Galacto-RGD in cancer patients. J Nucl Med 2005;46:1333–1341. [PubMed: 16085591]
53. Haubner R, Weber WA, Beer AJ, Vabulience E, Reim D, Sarbia M, Becker KF, Goebel M, Hein R, Wester HJ, Kessler H, Schwaiger M. Noninvasive visualization of the activiated $\alpha_v\beta_3$ integrin in cancer patients by positron emission tomography and [^{18}F]Galacto-RGD. PLOS Medicine 2005;2:e70, 244–252. [PubMed: 15783258]
54. Beer AJ, Grosu AL, Carlsen J, Kolk A, Sarbia M, Stangier I, Watzlowik P, Wester HJ, Haubner R, Schwaiger M. [^{18}F]Galacto-RGD positron emission tomography for imaging of $\alpha_v\beta_3$ expression on the neovasculature in patients with squamous cell carcinoma of the head and neck. Clin Cancer Res 2007;13:6610–6616. [PubMed: 18006761]
55. Wang L, Kim YS, Shi J, Zhai S, Jia B, Liu Z, Zhao H, Wang F, Chen X, Liu S. Improving tumor targeting capability and pharmacokinetics of ^{99m}Tc-labeled cyclic RGD dimers with PEG_4 linkers. Mol Pharm 2009;6:231–245. [PubMed: 19067525]
56. Shi J, Wang L, Kim YS, Zhai S, Liu Z, Chen X, Liu S. Improving tumor uptake and excretion kinetics of ^{99m}Tc-labeled cyclic Arginine-Glycine-Aspartic (RGD) dimers with triglycine linkers. J Med Chem 2008;51:7980–7990. [PubMed: 19049428]
57. Shi J, Wang L, Kim YS, Zhai S, Liu Z, Chen X, Liu S. Improving tumor uptake and pharmacokinetics of ^{64}Cu-labeled cyclic RGD dimers with triglycine and PEG_4 Linkers. Bioconj Chem Accepted.
58. Liu S, Edwards DS, Looby RJ, Harris AR, Poirier MJ, Rajopadhye M, Bourque JP, Carroll TR. Labeling cyclic glycoprotein IIb/IIIa receptor antagonists with ^{99m}Tc by the preformed chelate approach: Effects of chelators on properties of ^{99m}Tc-chelator-peptide conjugates. Bioconj Chem 1996;7:196–202.
59. Cai W, Rao J, Gambhir SS, Chen X. How molecular imaging is speeding up antiangiogenic drug development? Mol Cancer Ther 2006;5:2624–2633. [PubMed: 17121909]
60. Niu G, Chen X. Has molecular and cellular imaging enhanced drug discovery and drug development? Drugs in R&D 2008;9:351–368.

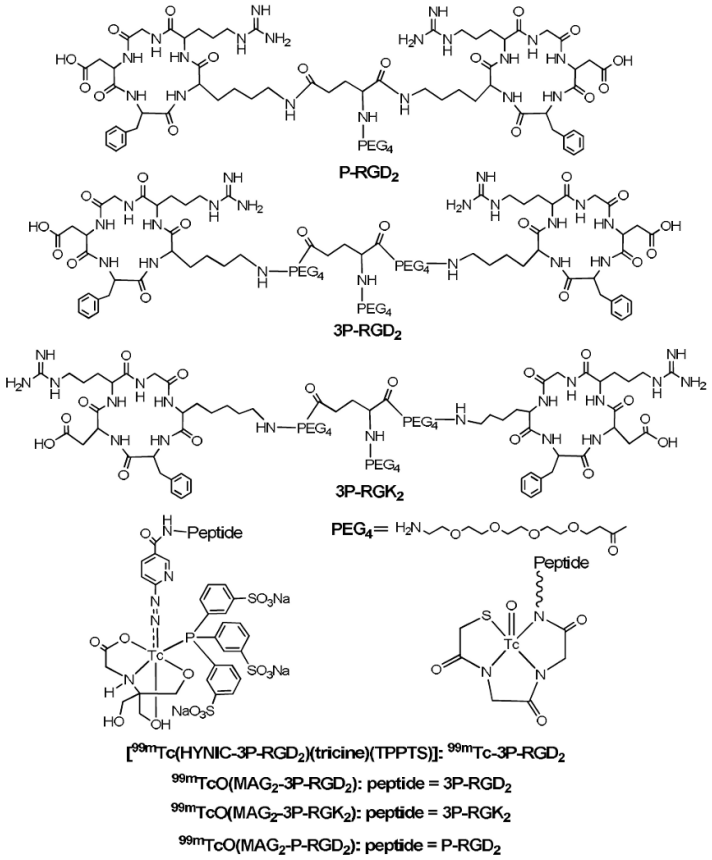

Figure 1.

Structures of bivalent cyclic RGD dimers (P-RGD_2 and 3P-RGD_2) and their ^{99m}Tc complexes: [^{99m}Tc(HYNIC-3P-RGD_2)(tricine)(TPPTS)] (^{99m}Tc-3P-RGD_2), ^{99m}TcO(MAG_2-P-RGD_2) and ^{99m}TcO(MAG_2-3P-RGD_2).

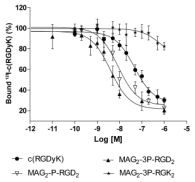

Figure 2.

The in vitro inhibition curve of ^{125}I-c(RGDyK) bound to integrin $\alpha_v\beta_3$ on U87MG human glioma cells by c(RGDyK), MAG_2-P-RGD_2, MAG_2-3P-RGD_2 and MAG_2-3P-RGK_2. Their IC_{50} values were calculated to be 46.6 ± 4.5, 8.6 ± 2.8, 3.9 ± 0.4 and 711 ± 128 nM, respectively.

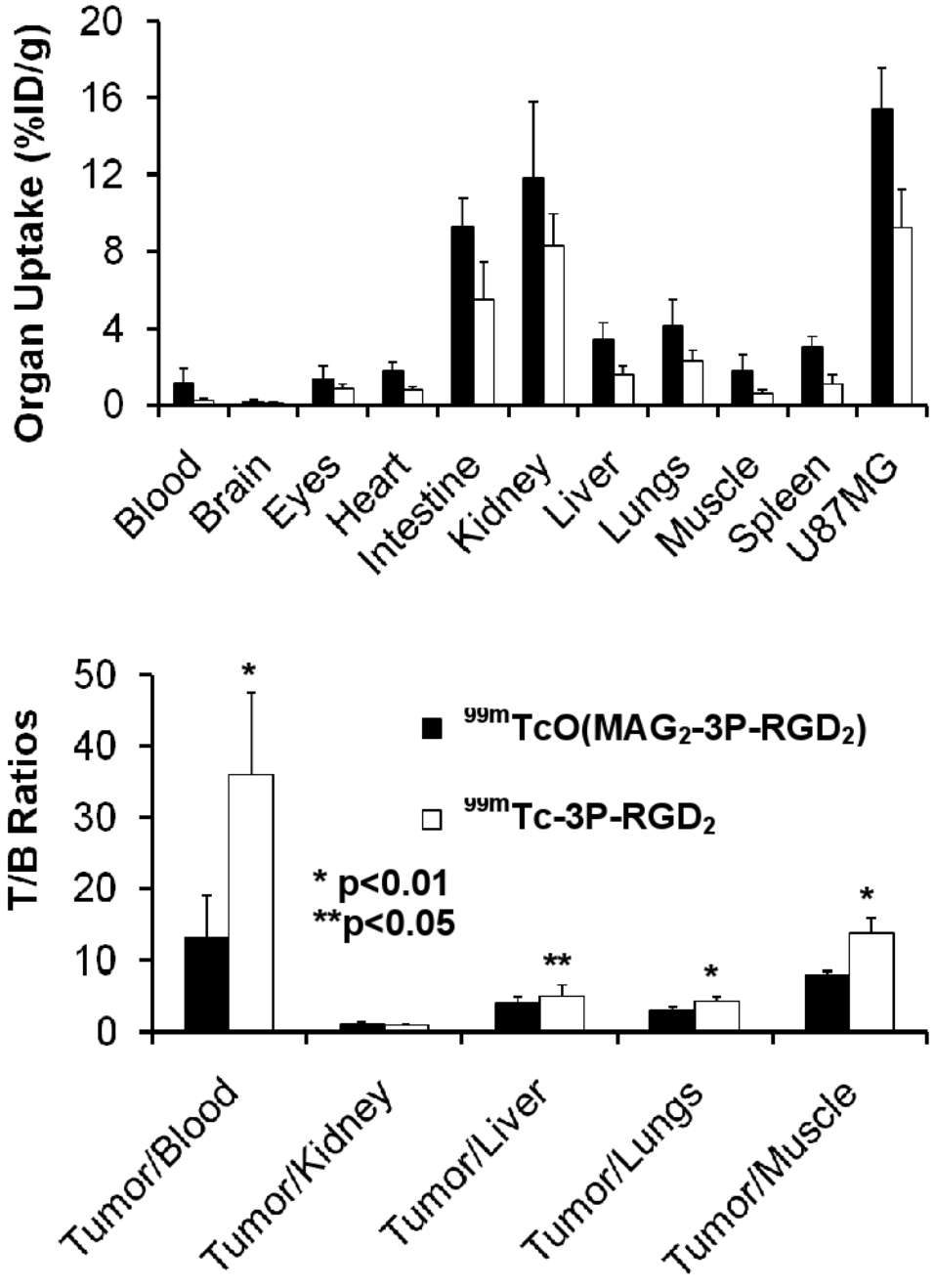

Figure 3.

Comparison of biodistribution data of ^{99m}TcO(MAG$_2$-3P-RGD$_2$) and ^{99m}Tc-3P-RGD$_2$ in the tumor, intestine, kidneys and liver from athymic nude mice (n = 5) bearing U87MG glioma xenografts at 60 min p.i.

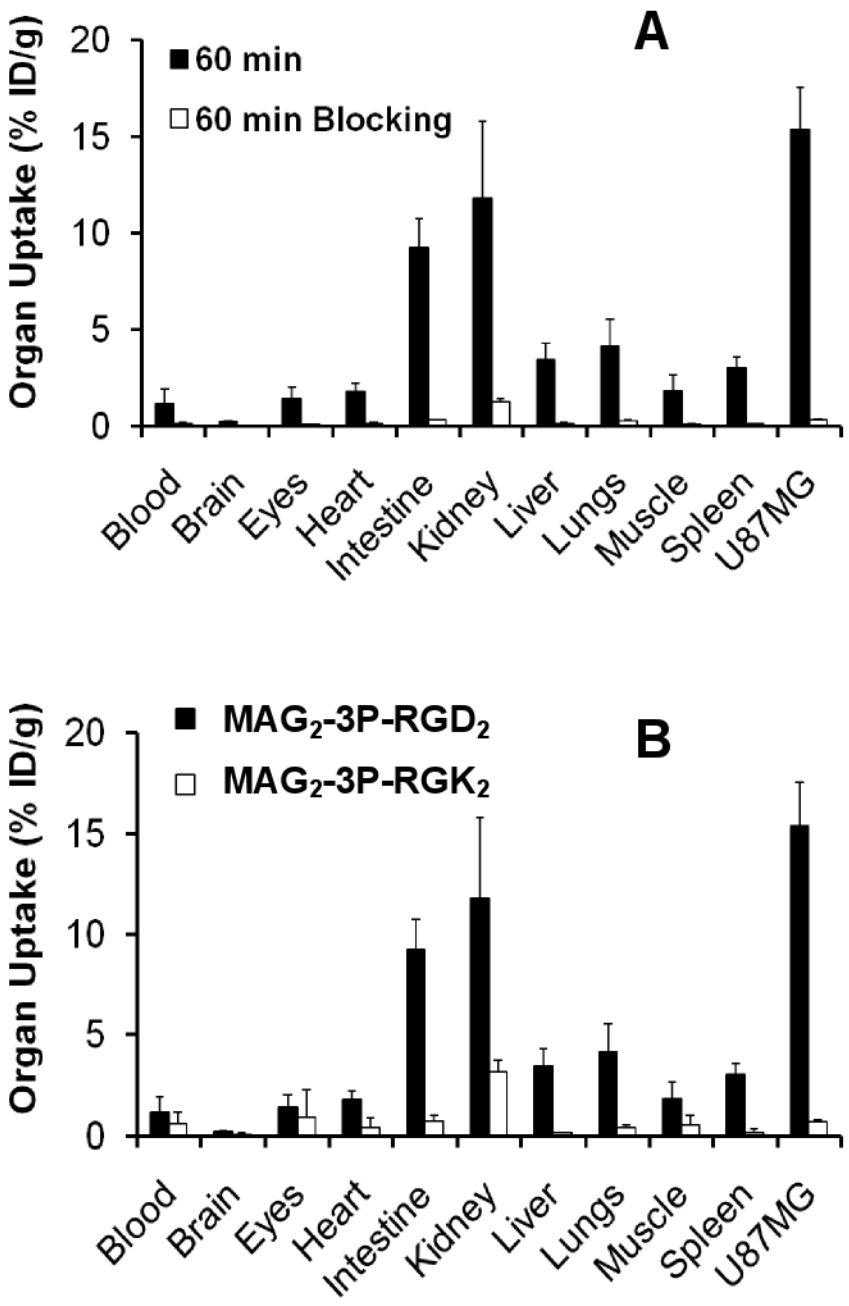

Figure 4.

A: Biodistribution data of ^{99m}TcO(MAG$_2$-3P-RGD$_2$) in athymic nude mice (n = 5) bearing U87MG human glioma xenografts in the absence/presence of excess E[c(RGDfK)]$_2$ (14 mg/kg or ~350 μg/mouse) at 60 min p.i. **B**: Direct comparison of biodistribution characteristics between ^{99m}TcO(MAG$_2$-3P-RGD$_2$) and ^{99m}TcO(MAG$_2$-3P-RGK$_2$) in athymic nude mice (n = 5) bearing U87MG human glioma xenografts at 60 min p.i.

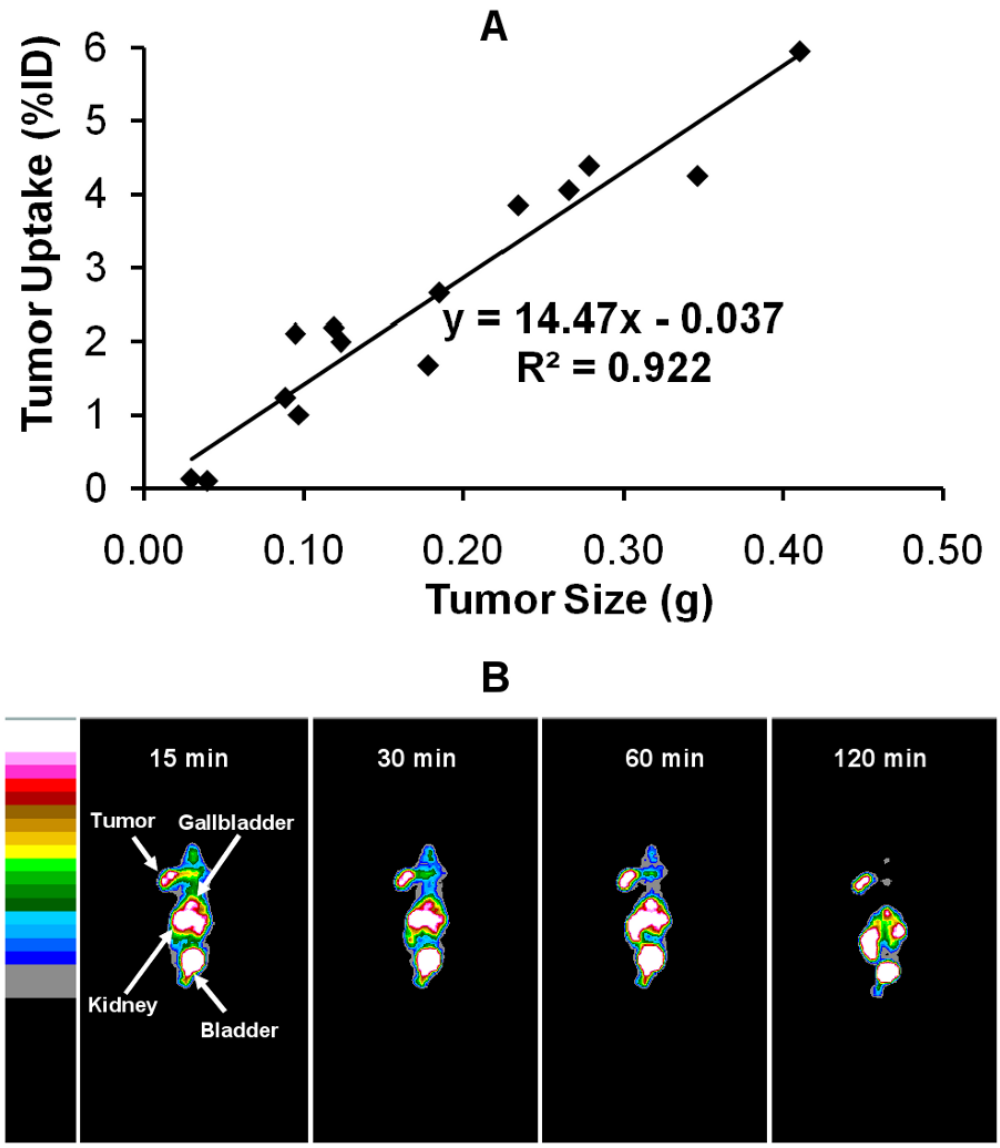

Figure 5.

A: the relationship between tumor size and tumor uptake for ^{99m}TcO(MAG$_2$-3P-RGD$_2$) at 120 min p.i. in the athymic nude mice (n = 14) bearing the U87MG glioma xenografts. The linear relationship between the tumor size and %ID tumor uptake suggests that ^{99m}TcO(MAG$_2$-3P-RGD$_2$) has the potential for noninvasive monitoring of tumor growth or shrinkage during anti-angiogenic therapy. **B**: planar images of the athymic nude mice (bearing U87MG glioma xenografts) administered with ~500 μCi of ^{99m}TcO(MAG$_2$-3P-RGD$_2$) at 15, 30, 60 and 120 min p.i. Arrows indicate the presence of the tumor, gallbladder, kidneys and bladder.

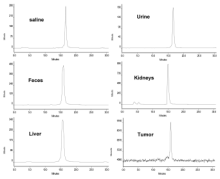

Figure 6.

Typical radio-HPLC chromatograms of ^{99m}TcO(MAG$_2$-3P-RGD$_2$) in saline before injection, urine, feces, kidney, liver and tumor at 120 min p.i. Slight variation in HPLC retention time was probably caused by the presence of 20% acetonitrile in the organ extract.

Table 1

HPLC retention time and log P values for ^{99m}Tc-labeled cyclic RGD peptides.

Compound	RCP (%)	RT (min)	Log P
^{99m}TcO(MAG$_2$-P-RGD$_2$)	> 95	17.0	- 3.30 ± 0.13
^{99m}TcO(MAG$_2$-3P-RGD$_2$)	> 90	16.9	-3.19 ± 0.15
^{99m}TcO(MAG$_2$-3P-RGK$_2$)	> 90	17.3	-2.40 ± 0.14
^{99m}Tc-3P-RGD$_2$	> 90	16.9	-4.35 ± 0.10*

* The log P value of −3.96 ± 0.05 was reported in our previous communication (55). These two values seem to be statistically significant; but they are within the experimental error of the assay.

Table 2

Biodistribution data of ^{99m}TcO(MAG$_2$-P-RGD$_2$) in athymic nude mice (n = 5) bearing U87MG human glioma xenografts.

	30 min	60 min	120 min
Blood	1.50 ± 0.64	0.85 ± 0.42	0.11 ± 0.02
Brain	0.45 ± 0.29	0.54 ± 0.55	0.09 ± 0.01
Eyes	2.21 ± 0.80	2.14 ± 0.55	0.94 ± 0.14
Heart	2.51 ± 1.13	1.60 ± 0.54	0.71 ± 0.10
Intestine	9.39 ± 2.92	5.25 ± 1.08	3.27 ± 1.14
Kidney	16.61 ± 5.52	9.95 ± 3.90	3.92 ± 0.60
Liver	4.25 ± 1.53	2.75 ± 0.76	1.47 ± 0.15
Lungs	5.41 ± 1.62	2.65 ± 0.57	2.28 ± 0.72
Muscle	3.33 ± 0.77	2.53 ± 1.10	1.12 ± 0.26
Spleen	3.52 ± 1.13	3.04 ± 1.09	1.25 ± 0.12
U87MG	9.63 ± 1.39	11.95 ± 1.90	5.90 ± 0.35
Tumor/Blood	8.53 ± 3.72	12.58 ± 2.60	46.62 ± 4.17
Tumor /Kidney	0.59 ± 0.08	1.15 ± 0.05	1.49 ± 0.28
Tumor /Liver	2.54 ± 0.68	2.98 ± 0.29	3.69 ± 0.58
Tumor /Lungs	1.95 ± 0.40	3.25 ± 1.13	2.93 ± 0.68
Tumor /Muscle	2.98 ± 0.35	4.20 ± 0.75	4.79 ± 0.54

Table 3

Biodistribution data of ^{99m}TcO(MAG$_2$-3P-RGD$_2$) in athymic nude mice (n = 5) bearing U87MG human glioma xenografts.

%ID/gram	30 min	60 min	120 min
Blood	1.62 ± 0.69	1.16 ± 0.78	0.42 ± 0.29
Brain	0.26 ± 0.07	0.21 ± 0.06	0.17 ± 0.07
Eyes	2.47 ± 1.34	1.40 ± 0.65	1.48 ± 0.77
Heart	2.40 ± 0.97	1.79 ± 0.45	1.05 ± 0.18
Intestine	10.99 ± 1.95	9.26 ± 1.50	6.58 ± 1.62
Kidney	16.35 ± 5.53	11.79 ± 3.98	6.07 ± 1.12
Liver	4.35 ± 1.51	3.45 ± 0.86	2.30 ± 0.23
Lungs	6.15 ± 1.93	4.17 ± 1.35	2.78 ± 0.49
Muscle	2.17 ± 0.35	1.82 ± 0.83	0.97 ± 0.24
Spleen	3.41 ± 1.12	3.02 ± 0.56	1.98 ± 0.14
U87MG	15.49 ± 5.55	15.36 ± 2.17	14.02 ± 2.20
Tumor/Blood	9.15 ± 2.51	13.52 ± 4.57	31.54 ± 10.23
Tumor /Kidney	0.98 ± 0.30	1.25 ± 0.36	2.01 ± 0.12
Tumor /Liver	3.49 ± 1.13	4.25 ± 0.88	5.81 ± 0.65
Tumor /Lung	2.51 ± 0.62	3.17 ± 0.60	4.95 ± 1.00
Tumor /Muscle	6.60 ± 1.25	8.34 ± 2.34	12.19 ± 1.07